DALTON
FULL PAPER

# Synthesis, spectroscopy and electrochemistry of tetrakis(μ-*N*,*N*′-diarylformamidinato)di(phenylethynyl)diruthenium(III) †,‡

**Chun Lin,[a] Tong Ren,*[,a] Edward J. Valente[b] and Jeffrey D. Zubkowski[c]**

[a] *Department of Chemistry, Florida Institute of Technology, Melbourne, FL 32901, USA*
[b] *Department of Chemistry, Mississippi College, Clinton, MS 39058, USA*
[c] *Department of Chemistry, Jackson State University, Jackson, MS 39217, USA*

The compounds $Ru_2[(XC_6H_4)NCHN(XC_6H_4)]_4(CCPh)_2$ (X = *p*-OMe, H, *p*-Cl, *m*-Cl, *m*-$CF_3$, 3,4-$Cl_2$ or 3,5-$Cl_2$) have been synthesized and characterized. These diamagnetic diruthenium(III) compounds display three (quasi)reversible redox couples: $Ru_2^{7+}$–$Ru_2^{6+}$ (A), $Ru_2^{6+}$–$Ru_2^{5+}$ (B) and $Ru_2^{5+}$–$Ru_2^{4+}$ (C). The electrode potential for each couple across the series linearly correlates with the Hammett constant (σ) of the substituent according to the following equation: $\Delta E_{\frac{1}{2}} = E_{\frac{1}{2}}(X) - E_{\frac{1}{2}}(H) = \rho(8\sigma)$ with ρ = 72.0, 92.4 and 80.5 mV for A, B and C, respectively, and the average HOMO–LUMO gap for the solvated diruthenium compounds is estimated as 1.35 eV. Consistent with the proposed ground-state configuration $\pi^4\delta^2\pi^{*4}$, a very long Ru–Ru bond (2.5554 Å) was revealed by an X-ray diffraction study of the compound with X = *p*-Cl, where unusual structural distortions in both the bridging and axial ligands were also observed. The origin of the distortions is attributed to the second-order Jahn–Teller effect, as elucidated from an MO analysis based on Fenske–Hall calculations.

The chemistry of metal–acetylide complexes has flourished during the last decade.[2] The successes in the synthesis of linear polymetallaynes containing middle and late transition metals[3] have inspired the notion of *molecular wires* based on the carbon-rich metallopolymers. In the search for model compounds for these polymers and optimization of the electronic communication along the polymer backbone, numerous alkynyl complexes, both mono- and oligo-nuclear (no direct metal–metal bond) have been synthesized and structurally characterized during the last few years.[2] Meanwhile, mononuclear alkynyl metal species have become important synthons/intermediates for organic chemists, where electrophilic activation at the β position of co-ordinated alkynyls is the key.[4] As a well documented example of such broad synthetic utility, the ruthenium–vinylidene intermediate derived from alkynyl ruthenium provides access to a variety of α,β-unsaturated carbonyl compounds.[5,6]

In contrast, there are few examples of metal–metal bonded dinuclear compounds bearing alkynyl groups, notably those of diruthenium[7,8] and dirhodium[9] with one or two axial phenylacetylides, and $M_2(PR_3)_4(CCR)_4$ (M = Mo or W) where the alkynyl groups co-ordinate at the equatorial positions.[10] Therefore, much remains to be explored concerning the nature of interactions between the alkynyl and the dinuclear core, *i.e.* what role alkynyl plays in determining the co-ordination geometry and electronic structures of the dinuclear core, how the dinuclear core activates the alkynyl, and the possible chemical transformation therein. We are particularly interested in converting axial alkynyl into axial vinylidene, a transformation common in the chemistry of mononuclear alkynyl compounds.[11] As the first step towards this goal, the current contribution reports the synthesis and characterization of the compounds **1**–**7**, and the linear free-energy relationship derived from an electrochemical study.

† Dedicated to the memory of Sir Geoffrey Wilkinson, one of the pioneers in diruthenium chemistry.
‡ Linear free-energy relationships in dinuclear compounds. Part 5.[1] *Supplementary data available*: UV/VIS, IR and NMR data, upper valence molecular orbitals and symmetry analysis. For direct electronic access see http://www.rsc.org/suppdata/dt/1998/571/, otherwise available from BLDSC (No. SUP 57330, 7 pp.) or the RSC Library. See Instructions for Authors, 1998, Issue 1 (http://www.rsc.org/dalton).

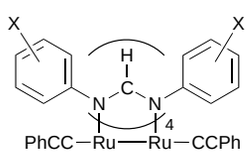


**X**
**1** *p*-OMe
**2** H
**3** *p*-Cl
**4** *m*-Cl
**5** *m*-$CF_3$
**6** 3,4-$Cl_2$
**7** 3,5-$Cl_2$

## Results and Discussion

### (*a*) Synthesis

New compounds **1** and **3**–**7** and the known compound **2** were prepared as described previously.[8] Consistent with the early report,[8] a 25-fold excess of PhCCLi not only results in complete substitution of the axial chloro ligand from the parent compound chlorotetrakis(μ-*N*,*N*′-diarylformamidinato)diruthenium(II,III) $Ru_2(form)_4Cl$.[1,12] but also shifts the equilibrium towards the formation of an anionic bis adduct, which was subsequently converted into the present compounds upon exposure to air, equation (1). Furthermore, it appears that the

$$Ru_2(form)_4(CCPh) + LiCCPh(excess) \rightleftharpoons [Ru_2(form)_4(CCPh)_2]^- \xrightarrow{O_2} Ru_2(form)_4(CCPh)_2 \quad (1)$$

electrophilicity of the diruthenium core increases with increase in the electron-withdrawing ability of the formamidinate substituent, and the compounds bearing strong electron-withdrawing substituents generally form faster and in higher yields than those with electron-releasing substituents, such as *p*-OMe.

### (*b*) Molecular structures

Well resolved $^1H$ and $^{13}C$ NMR spectra were recorded for compounds **1**–**7**, which imply diamagnetic ground states. A typical $^1H$ NMR spectrum consists of a downfield singlet for the methine proton (NCHN) and two sets of aromatic protons

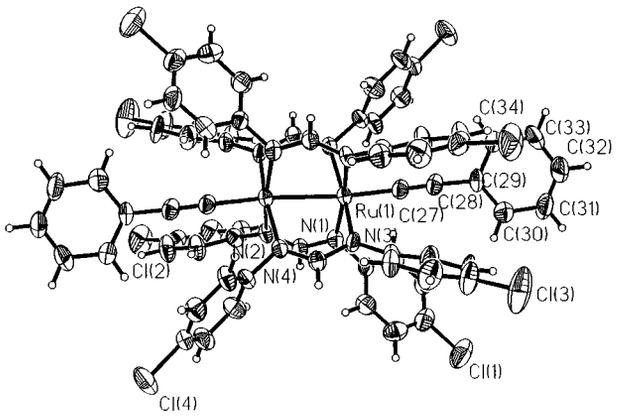


**Fig. 1** The ORTEP plot of compound **3**

**Table 1** Selected bond distances (Å) and angles (°) for compound **3**·2$C_6H_6$

| | | | |
|---|---|---|---|
| Ru(1)–Ru(1$^I$) | 2.5554(12) | N(1)–C(7) | 1.330(6) |
| Ru(1)–C(27) | 1.991(5) | N(2)–C(7) | 1.314(6) |
| Ru(1)–N(1) | 2.094(4) | N(3)–C(20) | 1.324(6) |
| Ru(1)–N(2) | 2.012(4) | N(4)–C(20) | 1.335(6) |
| Ru(1)–N(3) | 2.006(4) | C(27)–C(28) | 1.195(7) |
| Ru(1)–N(4) | 2.105(4) | | |
| | | | |
| C(27)–Ru(1)–N(1) | 88.0(2) | N(2)–Ru(1)–Ru(1$^I$) | 92.66(12) |
| C(27)–Ru(1)–N(2) | 100.4(2) | N(3)–Ru(1)–Ru(1$^I$) | 96.38(12) |
| C(27)–Ru(1)–N(3) | 101.1(2) | N(4)–Ru(1)–Ru(1$^I$) | 77.89(12) |
| C(27)–Ru(1)–N(4) | 85.6(2) | C(7)–N(1)–Ru(1) | 124.4(4) |
| N(3)–Ru(1)–N(1) | 86.6(2) | C(7)–N(2)–Ru(1$^I$) | 116.0(3) |
| N(2)–Ru(1)–N(1) | 169.8(2) | C(20)–N(3)–Ru(1) | 113.2(3) |
| N(3)–Ru(1)–N(2) | 86.1(2) | C(20)–N(4)–Ru(1$^I$) | 128.2(3) |
| N(3)–Ru(1)–N(4) | 172.3(2) | N(1)–C(7)–N(2) | 124.7(5) |
| N(2)–Ru(1)–N(4) | 89.0(2) | N(3)–C(20)–N(4) | 123.8(5) |
| N(1)–Ru(1)–N(4) | 97.5(2) | C(27)–Ru(1)–Ru(1$^I$) | 158.8(2) |
| N(1)–Ru(1)–Ru(1$^I$) | 81.06(12) | C(28)–C(27)–Ru(1) | 174.0(5) |

Symmetry transformation used to generate equivalent atoms: I: $-x+1, -y, -z+2$.

attributed respectively to the bridging ligands and axial phenylacetylides. The structural homogeneity among compounds **1**–**7** can be inferred from the simplicity and similarity in the pattern of $^1$H NMR spectra across the series.

The crystal structure of $Ru_2[(p\text{-}ClC_6H_4)NCHN(p\text{-}ClC_6H_4)]_4(CCPh)_2$ **3** has been determined, and an ORTEP[13] illustration of the molecule is shown in Fig. 1 while selected bond lengths and angles are listed in Table 1. The asymmetric unit consists of one half of **3** related to the other half *via* a crystallographic inversion center. Both the paddlewheel arrangement of bridging di(*p*-chlorophenyl)formamidinates and the axial ligation of phenylacetylides are obvious from Fig. 1. The Ru–Ru distance [2.5554(12) Å] indicates a weak bonding interaction between two ruthenium centres and is statistically identical to that in $Ru_2(PhNCHNPh)_4(CCPh)_2$ [2.556(1) Å],[8] but significantly longer than the Ru–Ru bond distances observed in $Ru_2(F_5ap)_4(CCPh)_2$ [2.451(1) Å; ($F_5$ap) = 2-(pentafluoroanilino)pyridinate],[14] $Ru_2(CH_2CMe_3)_6$ [2.311(3) Å] and $Ru_2(CH_2SiMe_3)_6$ [2.265(3) Å],[15] all diamagnetic diruthenium(III) compounds. Known paramagnetic $Ru_2^{6+}$ compounds also display distinctively short Ru–Ru bond lengths ranging from 2.30 to 2.35 Å.[16,17] Significant variations in both the Ru–Ru bond length and the magnetism are apparently manifested by the pseudo-degeneracy of the π* and δ* orbitals that is peculiar to the diruthenium species.[16] The ground-state configuration for **3** is $\pi^4\delta^2\pi^{*4}$, as suggested for $Ru_2^{6+}$ compounds with Ru–Ru distance longer than 2.45 Å.[17]

Most $M_2$(μ-formamidinate)$_4$ species possess an arrangement of bridging formamidinates in the $D_4$ point symmetry,[16] where all the M–N bonds are equivalent and both the M–N bond lengths and M–M′–N angles are statistically identical as shown

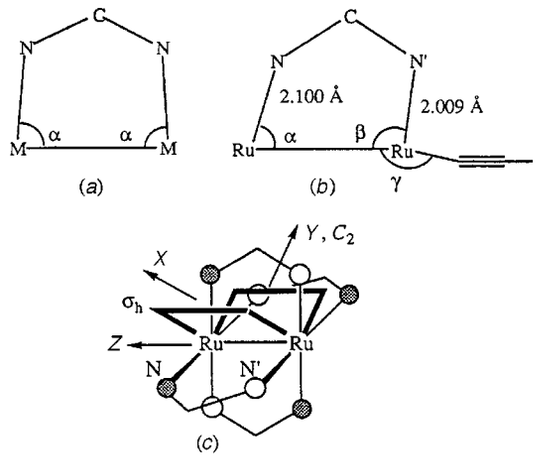


**Scheme 1** (*a*) Normal co-ordination geometry of formamidinates. (*b*) Observed distortion in compound **3**. (*c*) *cis*,*cis*-Head-to-tail arrangement in **3**, the symmetry elements of $C_{2h}$, and the master co-ordinates for model **8b**; the bold frames represent the *XZ* and *YZ* planes

in Scheme 1(*a*). Yet, the ligand arrangement in **3** deviates significantly from this norm. For each formamidinate, one of the nitrogen centers (N) is shifted towards the Ru–Ru bond to yield an acute Ru–Ru–N angle (α, average 79.5°) and an elongated Ru–N distance (average 2.100 Å), while the other (N′) is shifted away from the Ru–Ru bond to yield an obtuse Ru–Ru–N′ angle (β, average 94.6°) and a shortened Ru–N′ distance (2.009 Å), as shown in Scheme 1(*b*). Four formamidinates are arranged in a *cis*,*cis*-head-to-tail fashion which leads to an approximate $C_{2h}$ point symmetry for **3** [Scheme 1(*c*)]. Although the aryls attached to the N and N′ centers should be magnetically different, only one set of aryl protons is observed in the $^1$H NMR spectrum for each of the compounds, implying that the inequivalent Ru–N and Ru–N′ bonds are fluxional on the NMR time-scale. Interestingly, the aforementioned distortion does not induce much change in the eclipsed configuration of the $Ru_2N_8$ core, since the average N–Ru–Ru–N′ is only 8.1° in compound **3**, which is actually smaller than that for $Ru_2(form)_4(CCPh)$ (X = *m*-Cl) (12.1°).[18]

Concurrent with the distortion of the bridging formamidinates, the axial phenylacetylides are bent away from the Ru–Ru vector to yield a Ru–Ru–$C_\alpha$ angle (γ) of 158.8°. In contrast, all the monoalkynyl adducts of diruthenium(II,III) cores display a C≡C bond linear with the Ru–Ru vector (both Ru–Ru–$C_\alpha$ and Ru–$C_\alpha$–$C_\beta$ are 180°).[7,8,18] The origin of the distortions is possibly electronic and will be elaborated on the basis of MO calculations. While the Ru–$C_\alpha$ distances in compounds **3** [1.991(5) Å] and **2** [1.987(8) Å][8] are about the same, they are longer than the analogous distance for $Ru_2(F_5ap)_4(CCPh)_2$ [1.953(12) Å],[14] but shorter than that determined for the monoadducts (in the range of 2.02–2.08 Å).[7,8,18] Note that this trend is generally in accord with the order of the electrophilicity of the diruthenium cores.

### (*c*) Electrochemistry

Compounds **1**–**7** display three consecutive one-electron metal-based redox couples (2a)–(2c), as shown by their cyclic voltam-

$$Ru_2^{7+} + e^- \rightleftharpoons Ru_2^{6+} \quad \text{(reaction A)} \qquad (2a)$$

$$Ru_2^{6+} + e^- \rightleftharpoons Ru_2^{5+} \quad \text{(reaction B)} \qquad (2b)$$

$$Ru_2^{5+} + e^- \rightleftharpoons Ru_2^{4+} \quad \text{(reaction C)} \qquad (2c)$$

mograms in Fig. 2, which is consistent with the behavior established for **2**.[8] Examination of the electrochemical data obtained (Table 2) reveals that the redox couples are generally either reversible or quasi-reversible for most of the compounds.

**Table 2** Electrochemical and UV/VIS data for $Ru_2(form)_4(CCPh)_2$

| | X(σ) | | | | | | |
|---|---|---|---|---|---|---|---|
| | *p*-MeO (−0.27) | H [a] (0) | *p*-Cl (0.23) | *m*-Cl (0.37) | *m*-$CF_3$ (0.43) | 3,4-$Cl_2$ (0.60) | 3,5-$Cl_2$ (0.74) |
| $E_{\frac{1}{2}}$(A)/mV | 771 | 944 | 1085 | 1111 | 1219 | 1269 | 1413 [b] |
| ($\Delta E_p$, $i_{pb}/i_{pf}$) [c] | (97, 1.08) | (101, 0.90) | (153, 0.80) | (154, 0.95) | (166, 0.69) | (278, 0.93) | |
| $E_{\frac{1}{2}}$(B)/mV | −623 | −501 | −257 | −206 | −113 | 8 | 90 |
| ($\Delta E_p$, $i_{pb}/i_{pf}$) [c] | (94, 0.92) | (66, 0.99) | (119, 1.00) | (91, 0.99) | (159, 0.99) | (85, 0.99) | (69, 1.11) |
| $E_{\frac{1}{2}}$(C)/mV | −1578 | −1455 | −1251 | −1196 | −1170 | −1012 | −948 |
| ($\Delta E_p$, $i_{pb}/i_{pf}$) [c] | (131, 0.80) | (124, 0.91) | (122, 0.79) | (97, 0.63) | (156, 0.97) | (80, 0.87) | (69, 0.87) |
| $[E_{\frac{1}{2}}(A) - E_{\frac{1}{2}}(B)]$/mV | 1394 | 1445 | 1342 | 1317 | 1332 | 1261 | 1323 |
| $E_S(\pi^* \longrightarrow \delta^*)$ [d]/eV | 1.787 | 1.787 | 1.797 | 1.823 | 1.818 | 1.797 | 1.802 |

[a] Electrochemical data for this compound were reported in ref. 8(*a*), but were redetermined here to ensure a consistent experimental condition across the series. Only minor deviation was noticed. [b] Irreversible, reported as $E_{p,a}$ value. [c] Subscripts b and f indicate the backward (*anodic* for B and C, and *cathodic* for A) and forward (*anodic* for A, and *cathodic* for B and C) waves, respectively. [d] Singlet excitation energy based on the measured $\lambda(\pi^* \longrightarrow \delta^*)$/nm according to $E$/eV = $10^7/(8065.5\ \lambda)$.

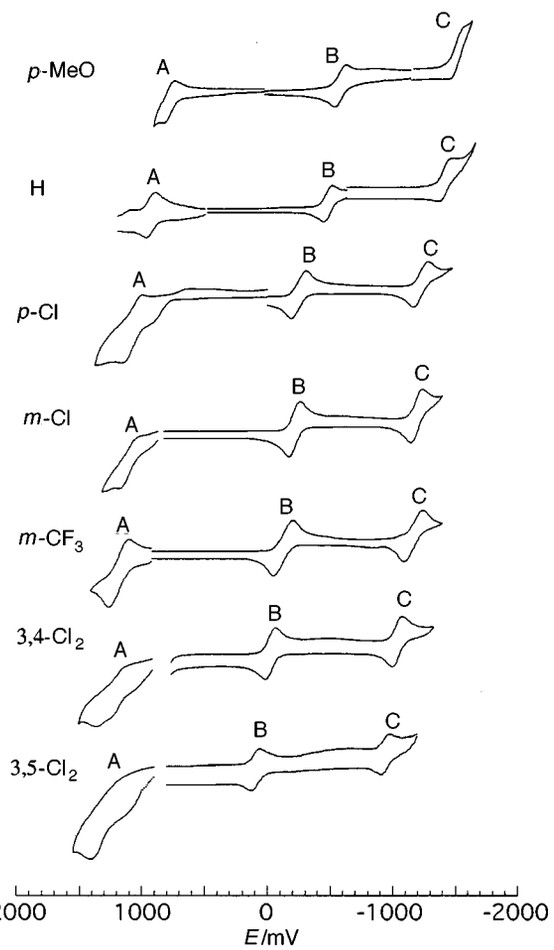


**Fig. 2** Cyclic voltammograms of compounds **1**–**7** recorded in $CH_2Cl_2$ with the scan rate of 100 mV $s^{-1}$

Similar to the trend observed for the formamidinate complexes of dimolybdenum(II),[19] dinickel(II),[20] and diruthenium(II,III),[1,18] the half-wave potential ($E_{\frac{1}{2}}$) for each couple shifts anodically with increasing σ across the series, which results in remarkable potential ranges: 642 mV for reaction A, 713 mV for B, and 630 mV for C. The substituent dependence of $E_{\frac{1}{2}}$ can be further quantified by linear least-squares fittings according to the Hammett equation (3),[21] where the reaction constants ρ

$$\Delta E_{\frac{1}{2}} = E_{\frac{1}{2}}(X) - E_{\frac{1}{2}}(H) = \rho(8\sigma) \quad (3)$$

(correlation coefficient) are 72.0 (0.990), 92.4 (0.993) and 80.5 (0.995) mV for reactions A, B and C, respectively.

Since the redox reactions A and B correspond respectively to the removal of an electron from the HOMO (π*) and the addition of an electron to the LUMO (δ*), the linear dependence of $E_{\frac{1}{2}}$ on σ clearly indicates that the energy levels of both the HOMO and LUMO are controlled by the phenyl substituent. When a molecule undergoes reversible one-electron oxidation and reduction, the relationship (4) exists where both $E$(LUMO)

$$E_{\frac{1}{2}}(\text{oxidation}) - E_{\frac{1}{2}}(\text{reduction}) = E(\text{LUMO}) - E(\text{HOMO}) \quad (4)$$

and $E$(HOMO) are referred to the solvated molecule.§[22] Hence the difference $E_{\frac{1}{2}}(A) - E_{\frac{1}{2}}(B)$ corresponds to the HOMO–LUMO gap for the *solvated* diruthenium species and the calculated values are also given in Table 2. There is no apparent correlation between the substituent constant σ and $E_{\frac{1}{2}}(A) - E_{\frac{1}{2}}(B)$ since a poor correlation coefficient (0.78) was obtained when fitting according to equation (3). The mean value (esd) of $E_{\frac{1}{2}}(A) - E_{\frac{1}{2}}(B)$ for compounds **1**–**7** is 1345(59) mV.

### (*d*) Electronic structures and electronic spectra

Observation of a significant distortion in the bridging formamidinates and the deviation of the Ru–Ru–$C_\alpha$ angle from linearity in both compounds **2**[8] and **3** prompts an examination of the electronic structure of these compounds based on Fenske–Hall calculations[23] of the model compounds **8a** and **8b** which share the same stoichiometric formula $Ru_2[HNC(H)NH]_4(C{\equiv}CH)_2$ but differ in the ligand geometry. While the distortions in both the bridging formamidinates and axial acetylides depicted in Scheme 2(*b*) were considered **8b** ($C_{2h}$ symmetry), these distortions were averaged in **8a**, where all the Ru–N bonds are equivalent, the C≡CH groups are collinear with the Ru–Ru vector, and the overall symmetry is $D_{4h}$. Information about the frontier orbitals and some valence MOs nearby is summarized in Table 3 for both **8a** and **8b**.

For model compound **8a** the frontier orbitals and other MOs with large ruthenium contribution (≥40%) are, in ascending order of energy, $7e_u[\pi(Ru{-}Ru)]$, $2b_{2g}[\delta(Ru{-}Ru)]$, $6e_g[HOMO, \pi^*(Ru{-}Ru)]$, $8a_{1g}[LUMO, \sigma^*(Ru{-}C)]$, $2b_{1u}[\delta^*(Ru{-}Ru)]$, which confirms the anticipated ground-state configuration $\pi^4\delta^2\pi^{*4}$.[17] Consistent with the long Ru–Ru distance observed, the MO calculation indicates that the δ bond is the only net Ru–Ru bond. The calculation also reveals that instead of forming a σ(Ru–Ru) bond, the $d_{z^2}$ orbitals from both ruthenium centers are involved in the Ru–$C_\alpha$ σ-bonding and -antibonding orbitals.

§ The error due to neglecting the difference in diffusion and activity coefficients for neutral, reduced and oxidized species is generally less than 10 mV.

**Table 3** Upper valence molecular orbitals for the model compounds $Ru_2[HNC(H)NH]_4(CCH)_2$

Model **8a**

| MO | *E*/eV | Assignment | Contributions[a] (%) |
|---|---|---|---|
| $2a_{1u}$ | 3.06 | π*(N–C–N) | N $p_\pi$ (42), $C_m$ $p_\pi$ (58) |
| $3b_{2g}$ | 3.04 | π*(N–C–N) | Ru $d_{xy}$ (10), N $p_\pi$ (42), $C_m$ $p_\pi$ (47) |
| $8e_u$ | 2.06 | π*(N–C–N) | N $p_\pi$ (41), $C_m$ $p_\pi$ (57) |
| $2b_{1u}$ | −5.68 | δ*(Ru–Ru) | Ru $d_{xy}$ (72), N $p_\pi$ (28) |
| $8a_{1g}$ | −6.75 | σ*(Ru–C), LUMO | Ru $(dsp)_\sigma$ (76), $C_\alpha$ $p_\sigma$ (19), N $(sp)_\sigma$ (4) |
| $6e_g$ | −7.41 | π*(Ru–Ru), HOMO | Ru $d_\pi$ (87), $C_\beta$ $p_\pi$ (10) |
| $2b_{2g}$ | −9.43 | δ(Ru–Ru) | Ru $d_{xy}$ (83), $C_m$ $p_\pi$ (17) |
| $7e_u$ | −10.23 | π(Ru–Ru) | Ru $d_\pi$ (82), $C_\beta$ $p_\pi$ (14) |
| $1a_{1u}$ | −11.43 | π(N–C–N) | N $p_\pi$ (100) |
| $5e_g$ | −12.45 | π(N–C–N) | N $p_\pi$ (96) |

Model **8b**

| MO | *E*/eV | Assignment | Contributions (%) |
|---|---|---|---|
| $17b_u$ | 5.94 | σ*(Ru–C) | Ru $(dsp)_\sigma$ (54), N $(sp)_\sigma$ (12), $C_\sigma$ $p_\sigma$ (20), $C_\beta$ p (10) |
| $12b_g$ | 4.39 | π*(N–C–N) | N $p_\pi$ (42), $C_m$ $p_\pi$ (58) |
| $17a_g$ | 4.21 | π*(N–C–N) | N $p_\pi$ (43), $C_m$ $p_\pi$ (49) |
| $12a_u$ | 3.47 | π*(N–C–N) | N $p_\pi$ (42), $C_m$ $p_\pi$ (57) |
| $16b_u$ | 3.15 | π*(N–C–N) | N $p_\pi$ (40), $C_m$ $p_\pi$ (54) |
| $16a_g$ | −4.55 | | Ru $d_{xz}$ (41), $p_z$ (36) |
| $15b_u$ | −5.99 | δ*(Ru–Ru), LUMO | Ru $d_{x^2-y^2}$ (70) |
| $11b_g$ | −7.80 | π*(Ru–Ru), HOMO | Ru $d_{yz}$ (84), $d_{xy}$ (3), $C_\beta$ $p_\pi$ (10) |
| $15a_g$ | −9.51 | δ(Ru–Ru) | Ru $d_{x^2-y^2}$ (73), $d_{xz}$ (8) |
| $14b_u$ | −9.76 | π(Ru–Ru) | Ru $d_{z^2}$ (15), $d_{xz}$ (61) |
| $14a_g$ | −9.94 | | Ru $d_{z^2}$ (28), $d_{xz}$ (29), $d_{x^2-y^2}$ (9) |
| $11a_u$ | −10.30 | π(Ru–Ru) | Ru $d_{yz}$ (70) |
| $10a_u$ | −11.72 | π(N–C–N) | N $p_\pi$ (90) |

[a] $C_\alpha$, $C_\beta$ and $C_m$ are the α, β carbons of acetylide and methine carbon of formamidinate, respectively.

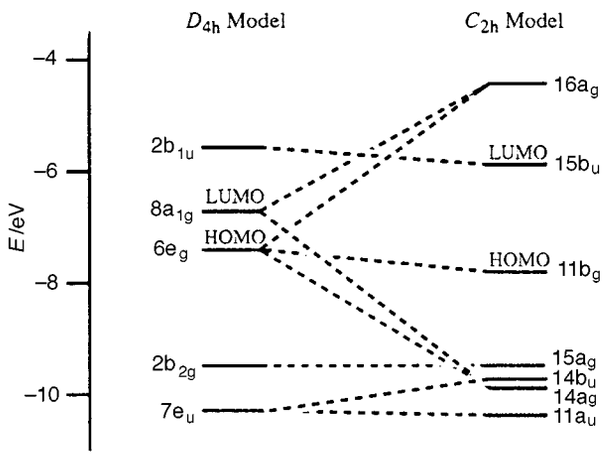


**Fig. 3** Orbital correlation diagram between model compounds **8a** and **8b**

However, the HOMO–LUMO gap for this highly symmetric model is merely 0.66 eV, which normally implies either weak paramagnetism or structural instability.

Although the distribution of occupied valence orbitals in the model compound **8b** is almost identical to that of **8a**, most of the orbitals are energetically stabilized in comparison. The HOMO orbital [π*(Ru–Ru)] has been stabilized by 0.40 eV, and the HOMO–LUMO(δ*) gap is enlarged to 1.81 eV. The increase in the HOMO–LUMO gap from **8a** to **8b** can be easily understood through the construction of an orbital correlation diagram (Fig. 3). In the $D_{4h}$ model (**8a**) orbital interaction between the HOMO ($6e_g$) and LUMO ($8a_{1g}$) is symmetry forbidden. Upon lowering the point symmetry to $C_{2h}$ in **8a** the HOMO splits into two orbitals transforming respectively as $a_g$ and $b_g$ (see Table 4), while the LUMO becomes an orbital of $a_g$ symmetry. Further mixing between the LUMO and the $a_g$ component of the HOMO yields both a significantly stabilized $14a_g$ (by 2.5 eV in comparison with $6e_g$) and a equally destabilized $16a_g$ (by 2.2 eV in comparison with $8a_{1g}$) molecular orbitals in **8b**. (Note that the non-crossing rule is observed in Fig. 3, since $15a_g$ in **8b** is originated from $2b_{2g}$ in **8a**). Reflecting extensive mixing, $14a_g$ in **8b** contains a significant contribution from Ru $d_{z^2}$ (part of $8a_{1g}$ in **8a**), while $16a_g$ in **8b** has the largest orbital contribution from Ru $d_{xz}$ (part of $6e_g$ in **8a**). As the result, the LUMO + 1 in **8a** ($2b_{1u}$) becomes the LUMO in **8b**, and the $b_g$ component of the HOMO in **8a** remains as the HOMO in **8b**. Thus, in order to remove the instability in **8a**, the molecule resolves to assume a much-distorted geometry, where the stabilization of the HOMO through HOMO–LUMO mixing becomes symmetry-allowed. Therefore, the compounds investigated are examples of second-order Jahn–Teller molecular systems.[24] It is noteworthy that the closed-shell paddlewheel compounds generally have a HOMO–LUMO gap much larger than the one for **8a**, and hence they are not subject to a second-order Jahn–Teller distortion.

**Table 4** Correlation between $D_{4h}$ (model **8a**) and $C_{2h}$ (model **8b**)

| $D_{4h}$ | $C_{2h}$ | $D_{4h}$ | $C_{2h}$ |
|---|---|---|---|
| $A_{1g}$ | $A_g$ | $A_{1u}$ | $A_u$ |
| $A_{2g}$ | $B_g$ | $A_{2u}$ | $B_u$ |
| $B_{1g}$ | $B_g$ | $B_{1u}$ | $B_u$ |
| $B_{2g}$ | $A_g$ | $B_{2u}$ | $A_u$ |
| $E_g$ | $A_g + B_g$ | $E_u$ | $A_u + B_u$ |

Inspection of the result for model **8b** also reveals the absence of an apparent $\pi^*_{xz}$(Ru–Ru) orbital. However, the sum of $d_{xz}$ character over all of the occupied $a_g$ (symmetry for $\pi^*_{xz}$) orbitals is about 51%, and thus an occupied $\pi^*_{xz}$ does exist. The ground-state configuration $\pi^4\delta^2\pi^{*4}$ is retained for **8b**.

General features of UV/VIS absorption spectra of the bis adducts in $CH_2Cl_2$ solutions include an intense peak around 540 nm and shoulders around 690, 505 and 420 nm, which are consistent with the spectrum reported earlier for **2**.[8] Based on the MO results, the peak at 540 nm and the shoulder around 690 nm are assigned to the dipole-allowed $\delta(15a_g) \longrightarrow \delta^*(15b_u)$ and $\pi^*(11b_g) \longrightarrow \delta^*$ transitions, respectively. Although the intensity of the absorption at 540 nm is higher than that for a typical d–d transition, it is not uncommon for diruthenium species due to 'intensity stealing' manifested by the significant orbital contribution from the N–C–N linkage to both the δ and δ* orbitals.[25] The high-energy shoulders around 505 and 420 nm are tentatively assigned as the LMCT from π(N–C–N) (such as $11a_u$, $10b_g$ and $13a_g$) to the δ*(Ru–Ru). The average *optical* HOMO–LUMO gap is 1.797(14) eV, which is significantly larger than that derived from the electrochemical study (1.345 eV). The discrepancy is due to the fact that the optical gap, or the singlet excitation energy, differs from the electrochemical gap by a term of $-J_{12}$(coulomb integral) + $2K_{12}$(exchange integral).[22]

### (*e*) Activation of C≡C bond

The C≡C bond in metal-bound alkynyls may be activated *via* either weakening of the σ($C_\alpha$–$C_\beta$) bond through the formation of a strong σ(M–$C_\alpha$) bond (inductive) or weakening of the π($C_\alpha$–$C_\beta$) bond through $d_\pi$–$p_\pi$($C_\alpha$) interaction (π-back don-

ation). Since the broad range of half-wave potentials implies a significant variation in the electron-richness of the $Ru^{III}_2$ core for compounds **1**–**7**, a substantial influence on the C≡C bond strength would be anticipated. However, the ν(C≡C) values across the series [mean 2100(2) $cm^{-1}$] show no substituent dependence at all. While in-depth understanding of such a substituent independence awaits more accurate theoretical modeling, a plausible explanation is that the inductive and π-back donation effects cancel each other.

## Conclusion

A facile synthesis of a series of diruthenium(III) compounds bearing two axial phenylacetylides in satisfactory yields is reported, which implies the general accessibility of this type of compound with other transition-metal centers. As the first example of linear substituent redox-tuning for dinuclear organometallic compounds, the linear free-energy relationship reported complements the early studies of dimolybdenum,[19] dinickel,[20] and diruthenium compounds.[1] In addition, the origin of unusual geometric distortions observed for diruthenium(III) paddlewheel compounds has been attributed to a second-order Jahn–Teller effect. The conversion of the reported compounds into the corresponding vinylidene compounds is being investigated. A complete list of IR and $^{13}C$ NMR data is provided in the supplementary data (SUP 57330).

## Experimental

All the chlorotetrakis(diarylformamidinato)diruthenium(II,III) compounds were prepared as previously described.[1] Phenylacetylene, lithium phenylacetylide and *n*-butyllithium [1.6 M in tetrahydrofuran (thf)] were from Aldrich. Tetrahydrofuran was distilled over sodium–benzophenone under a nitrogen atmosphere prior to use. Proton and $^{13}C$ NMR spectra were recorded on a Bruker AMX-360 spectrometer, with chemical shifts (δ) referenced to the residual $CHCl_3$ and the solvent $CDCl_3$, respectively, infrared spectra on a Nicolet system 550 (Magna series) FTIR spectrometer using KBr discs and UV/VIS spectra in $CH_2Cl_2$ with an IBM 9420 spectrophotometer. Cyclic voltammograms were recorded in 0.1 M $NBu_4BF_4$ solution ($CH_2Cl_2$, $N_2$-degassed) on a BAS CV-50W voltammetric analyzer with platinum working and auxiliary electrodes and a Ag–AgCl reference electrode. The ferrocenium–ferrocene couple (added as internal reference) was measured at 0.625 V under the experimental conditions.

### Synthesis

All the compounds were prepared by the following method: the parent compound chlorotetrakis(diarylformamidinato)-diruthenium(II,III)[1] (0.20 mmol) was dissolved/suspended in dry thf (30 $cm^3$) under argon. To this solution at 0 °C was added PhCCLi (10 mmol, freshly prepared by treating PhCCH with an equal amount of LiBu in dry thf at −78 °C under argon) with stirring, whereupon it immediately changed from dark green to dark red. After being stirred for 20 min, the reaction mixture was allowed to warm to room temperature and stirred under argon until it became yellowish brown. It was further stirred in the air for 30 min before the volatiles were removed under vacuum. The purple residue was dissolved in $CH_2Cl_2$ (10 $cm^3$), loaded onto a short plug of silica, then eluted with $CH_2Cl_2$. The solvent was removed from the purple fraction by bubbling air through it at ambient temperature. The crude product was further purified on a silica gel column with $CH_2Cl_2$–hexane as the eluent (the exact ratio for individual compounds is given below). Evaporation of solvents from the purple band yielded the crystalline product. (Note: while satisfactory yields were achieved with the PhCCLi prepared *in situ*, little or no products were isolated when the same procedure was repeated using the commercial PhCCLi reagent from Aldrich).

**$Ru_2$[(*p*-$MeOC_6H_4$)NCHN(*p*-$MeOC_6H_4$)]$_4$$(CCPh)_2$ 1.** Eluent: $CH_2Cl_2$. Yield: 5%. $^1H$ NMR: δ 8.17 (s, 4 H, NCHN), 7.09 (t, 4 H, $CCC_6H_5$, $^3J$ = 7.7), 6.84 (t, 2 H, $CCC_6H_5$, $^3J$ = 7.4), 6.77 (d, 16 H, phenyl ring of bridging ligand, $^3J$ = 8.8), 6.62 (d, 16 H, phenyl ring of bridging ligand, $^3J$ = 8.8), 6.35 (d, 4 H, $CCC_6H_5$, $^3J$ = 7.1 Hz) and 3.68 (s, 24 H, $OCH_3$). UV/VIS: $\lambda_{max}$/nm (ε/$M^{-1}$ $cm^{-1}$) 694 (sh), 574 (12 460), 507 (14 370) and 426 (sh). ν(C≡C): 2099 $cm^{-1}$.

**$Ru_2$(PhNCHNPh)$_4$$(CCPh)_2$ 2.** Eluent: $CH_2Cl_2$–hexane (9:1 v/v). Yield: 36%. $^1H$ NMR: δ 8.28 (s, 4 H, NCHN), 7.12–7.04 (m, 28 H, phenyl ring of bridging ligand and $CCC_6H_5$), 6.88–6.83 (m, 18 H, phenyl ring of bridging ligand and $CCC_6H_5$) and 6.28 (d, 4 H, $CCC_6H_5$, $^3J$ = 7.2 Hz). UV/VIS: $\lambda_{max}$/nm (ε/$M^{-1}$ $cm^{-1}$) 694 (sh), 534 (16 200), 510 (sh) and 416 (sh). ν(C≡C): 2101 $cm^{-1}$.

**$Ru_2$[(*p*-$ClC_6H_4$)NCHN(*p*-$ClC_6H_4$)]$_4$$(CCPh)_2$ 3.** Eluent: $CH_2Cl_2$. Yield: 73%. $^1H$ NMR: δ 8.21 (s, 4 H, NCHN), 7.22 (t, 4 H, $CCC_6H_5$, $^3J$ = 7.7), 7.11 (d, 16 H, phenyl ring of bridging ligand, $^3J$ = 8.6), 6.96 (t, 2 H, $CCC_6H_5$, $^3J$ = 7.4), 6.77 (d, 16 H, phenyl ring of bridging ligand, $^3J$ = 8.6) and 6.25 (d, 4 H, $CCC_6H_5$, $^3J$ = 7.2 Hz). UV/VIS: $\lambda_{max}$/nm (ε/$M^{-1}$ $cm^{-1}$) 690 (sh), 526 (17 310), 504 (sh) and 424 (sh). ν(C≡C): 2099 $cm^{-1}$.

**$Ru_2$[(*m*-$ClC_6H_4$)NCHN(*m*-$ClC_6H_4$)]$_4$$(CCPh)_2$ 4.** Eluent: $CH_2Cl_2$–hexane (1:3 v/v). Yield: 39%. $^1H$ NMR: δ 8.29 (s, 4 H, NCHN), 7.12–7.08 (m, 20 H, phenyl ring of bridging ligand and $CCC_6H_5$), 6.92 (s, 8 H, phenyl ring of bridging ligand), 6.89 (t, 2 H, $CCC_6H_5$, $^3J$ = 7.2), 6.77–6.73 (m, 8 H, phenyl ring of bridging ligand) and 6.40 (d, 4 H, $CCC_6H_5$, $^3J$ = 7.6 Hz). UV/VIS: $\lambda_{max}$/nm (ε/$M^{-1}$ $cm^{-1}$) 680 (sh), 533 (17 650), 506 (sh) and 419 (sh). ν(C≡C); 2099 $cm^{-1}$.

**$Ru_2$[(*m*-$F_3CC_6H_4$)NCHN(*m*-$F_3CC_6H_4$)]$_4$$(CCPh)_2$ 5.** Eluent: $CH_2Cl_2$–hexane (1:3 v/v). Yield: 52%. $^1H$ NMR: δ 8.38 (s, 4 H, NCHN), 7.41 (d, 8 H, phenyl ring of bridging ligand, $^3J$ = 7.8), 7.31 (t, 8 H, phenyl ring of bridging ligand, $^3J$ = 7.8), 7.11 (s, 8 H, phenyl ring of bridging ligand), 7.08 (d, 8 H, phenyl ring of bridging ligand, $^3J$ = 8.0), 7.03 (t, 4 H, $CCC_6H_5$, $^3J$ = 7.7), 6.86 (t, 2 H, $CCC_6H_5$, $^3J$ = 7.4) and 6.02 (d, 4 H, $CCC_6H_5$, $^3J$ = 7.5 Hz). UV/VIS: $\lambda_{max}$/nm (ε/$M^{-1}$ $cm^{-1}$) 682 (sh), 529 (14 380), 502 (sh) and 420 (sh). ν(C≡C): 2102 $cm^{-1}$.

**$Ru_2$[(3,4-$Cl_2C_6H_3$)NCHN(3,4-$Cl_2C_6H_3$)]$_4$$(CCPh)_2$ 6.** Eluent: $CH_2Cl_2$–hexane (3:2 v/v). Yield: 54%. $^1H$ NMR: δ 8.29 (s, 4 H, NCHN), 7.27 (d, 8 H, phenyl ring of bridging ligand, $^3J$ = 8.1), 7.19 (t, 4 H, $CCC_6H_5$, $^3J$ = 7.6), 7.03 (d, 8 H, phenyl ring of bridging ligand, $^5J$ = 1.9), 6.96 (t, 2 H, $CCC_6H_5$, $^3J$ = 7.4), 6.72 (dd, 8 H, phenyl ring of bridging ligand, $^3J$ = 8.4, $^5J$ = 2.0) and 6.29 (d, 4 H, $CCC_6H_5$, $^3J$ = 7.6 Hz). UV/VIS: $\lambda_{max}$/nm (ε/$M^{-1}$ $cm^{-1}$) 690 (sh), 549 (13 710), 510 (sh) and 420 (sh). ν(C≡C): 2099 $cm^{-1}$.

**$Ru_2$[(3,5-$Cl_2C_6H_3$)NCHN(3,5-$Cl_2C_6H_3$)]$_4$$(CCPh)_2$ 7.** Eluent: $CH_2Cl_2$. Yield: 20%. $^1H$ NMR: δ 8.34 (s, 4 H, NCHN), 7.19 (s, 8 H, phenyl ring of bridging ligand), 7.13 (t, 4 H, $CCC_6H_5$, $^3J$ = 7.6), 6.93 (t, 2 H, $CCC_6H_5$, $^3J$ = 7.4), 6.85 (s, 16 H, phenyl ring of bridging ligand) and 6.49 (d, 4 H, $CCC_6H_5$, $^3J$ = 7.5 Hz). UV/VIS: $\lambda_{max}$/nm (ε/$M^{-1}$ $cm^{-1}$) 688 (sh), 539 (12 890), 503 (sh) and 423 (sh). ν(C≡C): 2099 $cm^{-1}$.

### X-Ray crystallography

**Crystal data.** $C_{92}H_{70}Cl_8N_8Ru_2$ **3**·$2C_6H_6$, $M$ = 1773.30, monoclinic, space group $P2_1/n$, $a$ = 16.290(7), $b$ = 15.700(6), $c$ = 16.946(8) Å, β = 107.43(3)°, $U$ = 4135(3) $Å^3$, $Z$ = 2 (the molecule has crystallographic inversion symmetry), $D_c$ = 1.424 g $cm^{-3}$, Mo-Kα radiation, λ = 0.710 73 Å. μ(Mo-Kα) = 6.75 $cm^{-1}$, $F$(000) = 3608.

**Data collection and processing.** Data were measured at 294(2) K with a Siemens R3m/V automated diffractometer using ω scans on a small thin rhomboidal crystal which was wedged into a 0.2 mm glass capillary filled with mother liquor–mineral oil mixture. During the data collection, 8331 independent reflections were measured ($\theta \leqslant 26.3°$), of which 3267 were considered observed ($|F_o| > 4\sigma(|F_o|)$). No absorption correction was applied.

**Structure analysis and refinement.** All the non-hydrogen atoms were located with direct methods and refined with anisotropic vibrational terms. The final model included two ordered benzene molecules per complex. Positions of hydrogen atoms were calculated and assigned the isotropic thermal parameters $U(\mathrm{H}) = 1.2U_{eq}(\mathrm{C})$ for those of the complex and $U(\mathrm{H}) = 1.5U_{eq}(\mathrm{C})$ for those of benzenes. Full-matrix least-squares refinement on $F^2$ converged with $R1 = 0.0449$ and $wR2 = 0.0973$ for the observed reflections, and the maximum and minimum difference peaks were 0.349 and −0.387 e Å$^{-3}$, respectively. Crystallographic computations were performed with both SHELXS 86[26] and SHELXL 93.[27]

CCDC reference number 186/819.

See http://www.rsc.org/suppdata/dt/1998/571/ for crystallographic files in .cif format.

### Computation procedures

Fenske-Hall molecular orbital calculations[23] on the model compound $Ru_2[HNC(H)NH]_4(CCH)_2$ were performed on a VAXstation 4000 VLC. Basis functions used were generated by the numerical Xα atomic orbital program[28] in conjunction with an Xα-to-Slater basis program.[29] In order to simplify the analysis, aryls of both the bridging formamidinates and the axial phenylacetylides were replaced with hydrogen atoms, and the N–H and $C_\beta$–H distances were 1.00 and 1.05 Å, respectively. While the Ru–Ru, Ru–$C_\alpha$, $C_\alpha$–$C_\beta$ distances were kept at the experimental values, two models differing in the arrangement of the ligands were considered. In model compound **8a** all the independent Ru–N distances and Ru–Ru–N angles obtained from the X-ray diffraction study were averaged to give a single set of Ru–N (2.054 Å) and Ru–Ru–N (87.0°) values, and the acetylides were collinear with the Ru–Ru vector, which leads to a point symmetry of $D_{4h}$. The unique axis $C_4$ ($Z$) is along the Ru–Ru vector, while the $XZ$ and $YZ$ planes contain the Ru–Ru–N planes. In the second model (**8b**) two sets of Ru–N and Ru–Ru–N were used: 2.100 Å and 79.48°, and 2.009 Å and 94.52°, and the bridging ligands are in a *cis*-*cis*-head-to-tail arrangement to satisfy the $C_{2h}$ symmetry. Under this setting, $\sigma_h$ ($XZ$ plane) bisects the equivalent Ru–Ru–N planes while $C_2$ ($Y$) bisects the inequivalent Ru–Ru–N planes, and the $Z$ axis is along the Ru–Ru vector (see Scheme 1). While the description of most metal–metal bonding orbitals is the same as the conventional ones,[16] the δ interaction is between two $d_{x^2-y^2}$ orbitals instead of conventional $d_{xy}$ orbitals. Noting that the $C_2$ axis and $\sigma_h$ plane in the $C_{2h}$ point group correspond to the $C_2''$ axis and $\sigma_d$ plane in the $D_{4h}$ point group in the current setting, a correlation table between the irreducible representations of the two symmetry groups can be constructed (Table 4).

## Acknowledgements

This work is supported in part by the Petroleum Research Fund/ACS and the Florida Solar Energy Center (T. R.), and the Office of Naval Research (E. J. V. and J. D. Z.). We are grateful to the referees for suggesting the correlation/descending symmetry analysis of MO results, Dr. Judy Eglin for helpful discussion, and Dr. E. T. Smith for making the electrochemical apparatus available.

## References

1 Part 4, C. Lin, T. Ren, E. J. Valente, J. D. Zubkowski and E. T. Smith, *Chem. Lett.*, 1997, 753.
2 *Modern Acetylene Chemistry*, eds. P. J. Stang and F. Diederich, VCH, Weinheim, 1995; J. Manna, K. D. John and M. D. Hopkins, *Adv. Organomet. Chem.*, 1995, **38**, 79.
3 N. Hagihara, K. Sonogashira and S. Takahashi, *Adv. Polym. Sci.*, 1980, **40**, 149; Z. Atherton, C. W. Faulkner, S. L. Ingham, A. K. Kakkar, M. S. Khan, J. Lewis, N. L. Long and P. R. Raithby, *J. Organomet. Chem.*, 1993, **462**, 265; M. S. Khan, S. J. Davies, A. K. Kakkar, D. Schwartz, B. Lin, B. F. G. Johnson and J. Lewis, *J. Organomet. Chem.*, 1992, **424**, 87.
4 L. S. Hegedus, *Transition Metals in the Synthesis of Complex Organic Molecules*, University Science Books, Mill Valley, CA, 1994.
5 B. M. Trost, *Chem. Ber.*, 1996, **129**, 1313.
6 C. Bruneau and P. H. Dixneuf, *Chem. Commun.*, 1997, 507.
7 A. R. Chakravarty and F. A. Cotton, *Inorg. Chim. Acta*, 1986, **113**, 19.
8 (*a*) J. L. Bear, B. Han, S. Huang and K. M. Kadish, *Inorg. Chem.*, 1996, **35**, 3012; (*b*) J. L. Bear, B. Han and S. Huang, *J. Am. Chem. Soc.*, 1993, **115**, 1175.
9 C.-L. Yao, K. H. Park, A. R. Khokhar, M.-J. Jun and J. L. Bear, *Inorg. Chem.*, 1990, **29**, 4033.
10 D. K. John, S. J. Geib and M. D. Hopkins, *Organometallics*, 1996, **15**, 4357 and refs. therein.
11 A. H. Hill, in *Comprehensive Organometallic Chemistry II*, Pergamon, Oxford, 1995, vol. 7.
12 F. A. Cotton and T. Ren, *Inorg. Chem.*, 1995, **34**, 3190.
13 C. K. Johnson, ORTEP, Report ORNL-5138, Oak Ridge National Laboratory, Oak Ridge, TN, 1976.
14 Y. Li, B. Han, K. M. Kadish and J. L. Bear, *Inorg. Chem.*, 1993, **32**, 4175.
15 R. P. Tooze, G. Wilkinson, M. Motevalli and M. B. Hursthouse, *J. Chem. Soc.*, *Dalton Trans.*, 1986, 2711.
16 F. A. Cotton and R. A. Walton, *Multiple Bonds between Metal Atoms*, Oxford University Press, Oxford, 1993.
17 F. A. Cotton and A. Yokochi, *Inorg. Chem.*, 1997, **36**, 567.
18 C. Lin, T. Ren, E. J. Valente and J. D. Zubkowski, unpublished work.
19 C. Lin, J. D. Protasiewicz, E. T. Smith and T. Ren, *Inorg. Chem.*, 1996, **35**, 6422; *J. Chem. Soc.*, *Chem. Commun.*, 1995, 2257.
20 C. Lin, J. D. Protasiewicz and T. Ren, *Inorg. Chem.*, 1996, **35**, 7455.
21 P. Zuman, *The Elucidation of Organic Electrode Processes*, Academic Press, New York, 1969.
22 R. O. Loutfy and R. O. Loutfy, *Can. J. Chem.*, 1976, **54**, 1454.
23 M. B. Hall and R. F. Fenske, *Inorg. Chem.*, 1972, **11**, 768.
24 T. A. Albright, J. K. Burdett and M.-H. Whangbo, *Orbital Interactions in Chemistry*, Wiley, New York, 1985, pp. 95–97.
25 F. A. Cotton and T. Ren, *Inorg. Chem.*, 1991, **30**, 3675.
26 G. M. Sheldrick, SHELXS 86, Program for Crystal Structure Determination, University of Göttingen, 1986.
27 G. M. Sheldrick, SHELXL 93, Program for Refinement of Crystal Structure, University of Göttingen, 1993.
28 B. E. Bursten and R. F. Fenske, *J. Chem. Phys.*, 1977, **67**, 3138; B. E. Bursten, J. R. Jensen and R. F. Fenske, *Chem. Phys.*, 1978, **68**, 3320.
29 F. Herman and S. Skillman, *Atomic Structure Calculations*, Prentice-Hall, Englewood Cliffs, NJ, 1963.

*Received* 26*th August* 1997; *Paper* 7/06190K